CrossMark

A particle-tracking technique for spatial and temporal interpolation of satellite images applied to Lake Superior chlorophyll measurements

Pengfei Xue [a,b,*], David J. Schwab [a,c,d], Reid W. Sawtell [d], Michael J. Sayers [d], Robert A. Shuchman [a,d], Gary L. Fahnenstiel [a,c,d]

[a] *Great Lakes Research Center, Michigan Technological University, Houghton, MI, United States*
[b] *Department of Civil and Environmental Engineering, Michigan Technological University, Houghton, MI, United States*
[c] *University of Michigan, Water Center, University of Michigan, Ann Arbor, MI, United States*
[d] *Michigan Tech Research Institute, Michigan Technological University, Ann Arbor, MI, United States*

A B S T R A C T

Ocean color satellite-derived estimates of water properties are generally discontinuous in spatial and temporal coverage due to cloud cover. We describe a novel method for providing an estimate of continuous distribution of a satellite-derived water property, chlorophyll concentration in Lake Superior. The method uses calculated wind-driven lake circulation from a hydrodynamic model to estimate the evolution of the chlorophyll concentration field between available imagery. This new technique considers hydrodynamic effects by integrating a property-carrying particle model (PCPM) and an Eulerian concentration remapping approach. The PCPM interpolation method uses computational tracer particles that move with the calculated lake currents to represent the chlorophyll field. The concentration associated with each particle is dynamically adjusted toward the satellite-derived chlorophyll field at times and locations where imagery is available and produces a spatially and temporally continuous estimate of the chlorophyll concentration field. One of the important characteristics revealed from the analysis is the seasonally-dependent and region-specific chlorophyll concentration, which is significantly controlled by seasonal hydrodynamic conditions in Lake Superior. Analysis suggests that without adding extra sampling cost, moving a few sampling locations from offshore water to sample the embayments and southern coasts can provide more accurate characterization of the spatial pattern of chlorophyll concentration in Lake Superior. Furthermore, we found that Lake Superior chlorophyll concentrations do not appear to have changed significantly over the past 12 years and likely only slightly or not at all over the last 50 years, which differs from that in the other upper Great Lakes.

© 2017 International Association for Great Lakes Research. Published by Elsevier B.V. All rights reserved.

Introduction

In large ecosystems such as the Laurentian Great Lakes, field measurements of water quality parameters are generally extremely limited in terms of temporal and spatial coverage (e.g., Scavia et al., 1986; Lehman, 1988; Makarewicz and Bertram, 1991; Johengen et al., 1994). For example, in Lake Superior with over 31,000 miles^2 of surface area, water quality trends are typically assessed by sampling 18 stations twice per year (April and August, GLNPO/EPA). Recently, to improve on the obvious temporal limitations of limited field sampling, remote sensing has been used to determine lake-wide trends in water quality parameters such as chlorophyll *a* (Barbiero et al., 2011; Warner and Lesht, 2015; Fahnenstiel et al., 2016). However, remote sensing of key parameters is not without limitations. Because satellite remote sensing

depends on clear skies in regions such as the Great Lakes where cloudy conditions can dominate during certain periods, only limited remote sensing observations are possible. For example, for the period of November 1, 2007 through March 31, 2008, a period of 5 months, not one 'clear' remote sensing image (defined as 75% over lake coverage) was observed in Lake Superior. Thus, although remote sensing has allowed for increased spatial sampling of water quality parameters, its limited ability to provide resolution on important temporal scales may diminish its application.

But, application of statistical or interpolation techniques may provide improved remote sensing products. In the Great Lakes there has previously been demonstrated success using traditional spatio-temporal interpolation techniques for satellite-derived images of surface water temperature as demonstrated by the Great Lakes Surface Environmental Analysis (GLSEA) product (Schwab et al., 1999). While this technique has proven to be extremely useful for some physical fields like temperature, we found that it was inadequate for biogeochemical

* Corresponding author.
  E-mail address: pexue@mtu.edu (P. Xue).

fields with higher degrees of spatio-temporal variability than surface water temperature. Other approaches need to be explored to improve the resolution of remotely sensed biogeochemical properties.

In this paper, we will introduce a new data assimilation technique, which combines remote sensing information with information about water movement from hydrodynamic models. There have been considerable advances in hydrodynamic modeling of coastal waters, to the point where accurate depictions of short-term and seasonal circulation patterns are routinely available. Since 2002, Lake Superior has been part of the National Oceanic and Atmospheric Administration's (NOAA) operational Great Lakes Coastal Forecasting System (GLCFS), which is built on a version of the Princeton Ocean Model (POM) for each of the Great Lakes (Schwab and Bedford, 1994). Since the development of GLCFS, there have been continuous advances in hydrodynamic modeling for Lake Superior (Bennington et al., 2010; White et al., 2012; Dupont et al., 2012; Xue et al., 2015) along with the other four Lakes. More recently, the unstructured grid Finite Volume Community Ocean Model (FVCOM) has been applied to the Great Lakes (Anderson and Schwab, 2013; Xue et al., 2015; Xue et al., 2017). With its promising performance, the FVCOM model is currently being used by NOAA for operational forecasting in several coastal regions and is scheduled to replace the Princeton Ocean Model in NOAA's GLCFS.

The motivation for the current study is to provide improved spatial and temporal coverage for remotely-sensed estimates of water quality parameters in a large ecosystem using a new combined hydrodynamic modeling/remote sensing approach. This new approach is critical because it provides a complete spatial and temporal remote sensing product overcoming many previous observational limitations. For example, in order to validate remote sensing algorithms for an increasingly complex array of biogeophysical parameters, it is becoming more important to generate values of the satellite-derived parameters for locations and times when ground truth is available, but satellite imagery may not be available. The interpolated parameter values can provide a valuable supplement to the relatively rare coincident ground truth/remote sensing data. Moreover, there is considerable value to a continuous spatio-temporal approximation of a satellite-derived biogeophysical parameter in terms of the types of geospatial analysis that can be utilized. One example is the decorrelation time analysis described later in this paper. Another advantage of the continuous fields is the ability to generate continuous parameter time series at any location in the field, as well as continuous time series of complete spatial averages. Finally, continuous spatio-temporal estimates of biogeochemical parameters will also be useful for examining biological processes with much greater spatial and temporal resolution compared to in situ measurements at sampling stations and intermittent and incomplete satellite imagery records. And, as improvements are made in coupled models of lake physics and ecology, continuous parameter fields will be increasingly useful for calibration, validation, and assimilation of future products.

There are typically two distinct approaches used to obtain estimates of a continuous spatio-temporal parameter field from incomplete data, which are based respectively on Eulerian and Lagrangian models. The first approach is to use a soluble tracer-based model to represent transport and mixing in a Eulerian framework, such that the tracer concentration field (C) is calculated using the mass conservation equation:

$$\frac{\partial DC}{\partial t} + \frac{\partial DuC}{\partial x} + \frac{\partial DvC}{\partial y} + \frac{\partial DwC}{\partial z} - \frac{1}{D}\frac{\partial}{\partial z}\left(K_h \frac{\partial C}{\partial z}\right) - DF_c = C_{source} - C_{sink} \quad (1)$$

where D is the total water depth, u, v, and w are the x, y and z components of the water velocity, K_h is the vertical thermal diffusion coefficient, F_c is the horizontal diffusion term, and C_{source} and C_{sink} represents the sources and sinks of C. This approach has been widely used in ocean modeling communities (Chen et al., 2008; Xue et al., 2009). Such a tracer-based model usually uses the same numerical approach as is used for the salinity equation in hydrodynamic models with the addition of source and sink terms. The tracer-based model

requires its model grid to match the hydrodynamic model grid (otherwise excessive interpolations for each grid and each time step are required and often significant interpolation-induced errors would occur). Such a requirement often means different hydrodynamic models come along with their own version of the tracer model, and different configurations of the tracer model will be required even in order to match different hydrodynamic model configurations.

The second approach, which we adopted here, is based on a Lagrangian particle-tracking model. Lagrangian models follow the trajectories of discrete tracer particles, as they are tranported by the currents. Commonly the tracer particles represent discrete units of mass and the concentration field is proportional to their local spatial density. What is unique in our approach is that we have developed a property-carrying particle model (PCPM, details described in the next section) that will estimate the domain properties (in this case, the chlorophyll concentration) using the particle-tracking trajectories generated from a traditional Lagrangian particle-tracking model, but with a time-varying concentration value associated with individual particles. The advantages of this approach is the simplicity of code construction, the efficiency of computation and freedom of model configuration as our model is constructed in a way that completely independent of the hydrodynamic model configuration and particle-tracking models. This shall be elucidated in the full description of the PCPM in the next section.

Methods

MODIS Ocean Color data

This study uses the Color Producing Agents Algorithm (CPA-A) to derive chlorophyll estimates from remotely sensed ocean color satellite data (Shuchman et al., 2013). The algorithm takes Remote Sensing Reflectance (Rrs) and produces Chlorophyll (Chl), Suspended Mineral (SM), and Dissolved Organic Compound (DOC) concentrations as output by optimizing a set of non-linear equations that relate component concentrations to signal spectra using a hydro-optical model. The Rrs abbreviation is specific to Ocean Color remote sensing, the premise being that Reflectance, R, can be computed in many different ways (often denoted in the subscript of R), here we use Remote Sensing (hence the rs subscript) Reflectance. MODIS Aqua Level 2 data, the standard atmospherically corrected output available through NASA Ocean Color Web (Software version 6.5.7, processed in 2012), were used as input to the algorithm. The CPA Algorithm offers several advantages over the standard chlorophyll product provided by Ocean Color, including a modest gain in retrieval accuracy as well as the production of SM and DOC concentrations which could also be used with the PCPM interpolation. Additionally the CPA-A produces for each 1 km^2 pixel, estimates of the light irradiance diffuse attenuation coefficient (Kd), chromophoric dissolved organic matter (CDOM), and photic zone depth, water optical parameters, which also could be used with the PCPM interpolation. Further details about the validation and use of the CPA-A Algorithm in the Great Lakes Region can be found in Shuchman et al. (2013) and Fahnenstiel et al. (2016).

The standard MODIS level 2 images include a set of output flags indicating conditions at each pixel. These flags were used to exclude land pixels (LAND), cloud/ice pixels (CLDICE), high-sensor view zenith angle (HISATZEN) and pixels likely containing straylight (STRAYLIGHT) contamination from nearby clouds or from the shoreline. While excluding straylight contaminated pixels results in a considerable loss of observable lake surface (~6%), predominantly in the nearshore area, the chlorophyll estimates suffer under such conditions and so their elimination is a net positive to the quality of the final result. The number of pixels rejected from HISATZEN is variable scene-to-scene as this flag simply removes the edges of each MODIS swath where long atmospheric path lengths are present (i.e. imperfect atmospheric correction), thus if part of the lake is in this region those corresponding pixels are removed. The number of pixels rejected by CLDICE is highly variable on

short time scales (days) due to rapidly changing weather patterns and ice conditions in the Great Lakes region, but is generally consistent with the 50–60% average overwater cloudiness during the April–October period reported by Ackerman et al. (2013).

Hydrodynamic modeling

The hydrodynamic model used in this study is FVCOM (Finite Volume Community Ocean Model) (Chen et al., 2006). FVCOM is an unstructured-grid, finite-volume, three-dimensional (3-D) primitive equation ocean model with a generalized, terrain-following coordinate system in the vertical and a triangular mesh in the horizontal. The unstructured grid can be designed to provide a customized variable resolution to both coastline and bathymetry. FVCOM has been used in numerous applications to estuaries, coastal oceans, and the Great Lakes (Xue et al., 2009; Anderson and Schwab, 2013; Xue et al., 2015; Xue et al., 2017). The Lake Superior FVCOM model is configured with a very high horizontal resolution of ~100 m around islands and complex shoreline features, a medium resolution of 200–500 m along the rest of the coast and nearshore region, and a moderate resolution of ~2 km in offshore areas, resulting in a total of ~65,000 model elements (Fig. 1a). Each model element uses 40 evenly spaced vertical sigma-coordinate

layers with a vertical resolution of <1 m in the coastal region and 2–5 m offshore.

The surface boundary condition of FVCOM consists of momentum and heat flux at each surface mesh element. The momentum and heat fluxes are calculated internally in FVCOM using surface meteorological data from the Climate Forecast System Reanalysis (CFSR, NCAR, 2015) and the internally calculated water temperature. As a global, high resolution, coupled atmosphere-ocean-land surface-sea ice system, the CFSR was designed to provide the best estimate of the state of these coupled domains by including: (1) coupling of atmosphere and ocean during the generation of the 6 h guess field, (2) an interactive sea-ice model, and (3) assimilation of satellite radiances by the Grid-point Statistical Interpolation scheme and all available conventional and satellite observations. Preliminary analysis of the CFSR output indicates a product far superior in most respects to the reanalysis of the mid-1990s (Saha et al., 2010).

The CFSR meteorological output is used as the physical forcing for Lake Superior FVCOM model. The CFSR forcing is retrieved at hourly temporal resolution and ~20 km horizontal resolution from the gridded reanalysis data. The hydrodynamic simulation driven by CFSR forcing for Lake Superior was shown to provide robust simulations of the circulation patterns and thermal structure, mainly due to its accurate
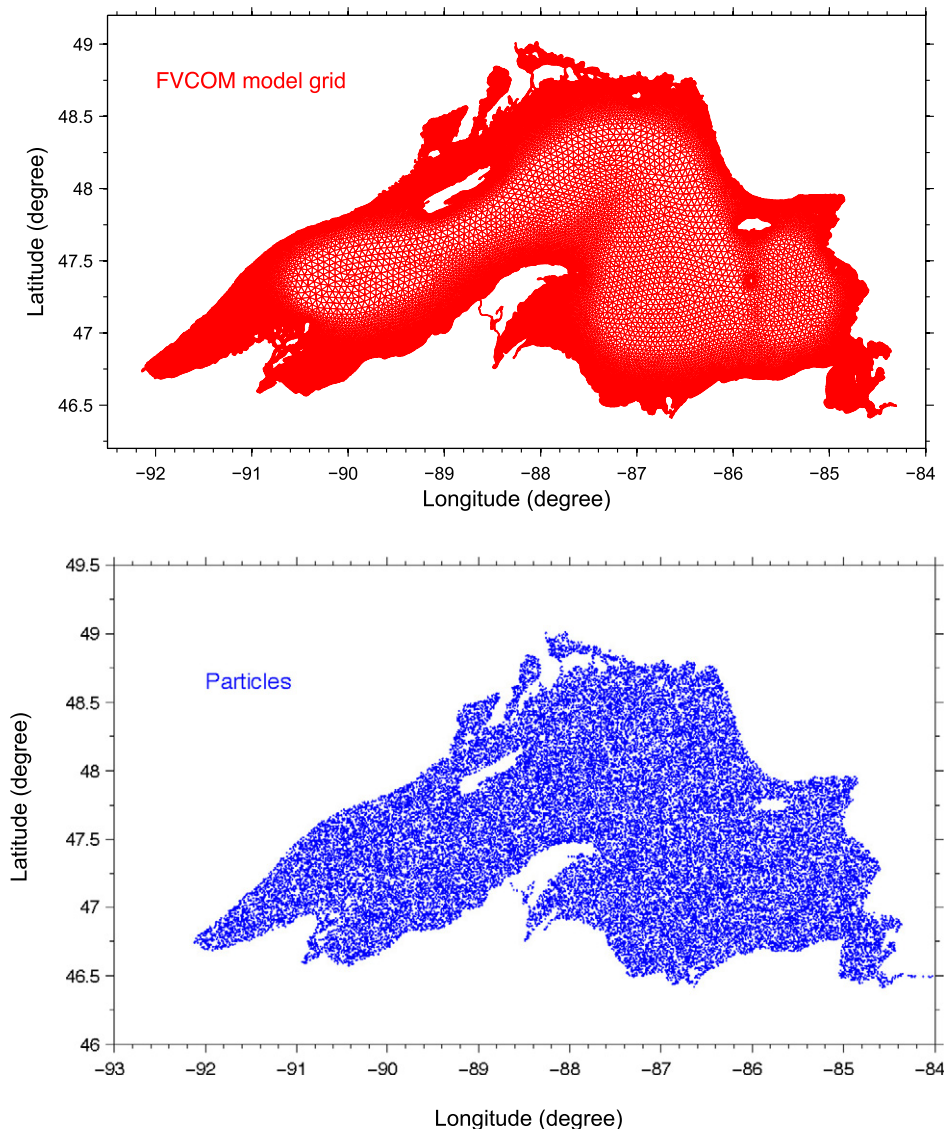

Fig. 1. Hydrodynamic model grid and particle initial distribution.

representation of wind pattern and radiation fields (Xue et al., 2015). With a focus on spatial and temporal estimates of chlorophyll fields, the model is applied to Lake Superior for the ice-free seasons of 2002–2013. The model configuration follows Xue et al. (2015). Each year begins with a 1-month spin-up starting on March 1 and runs continuously to December 31.

Calculation of chlorophyll fields

Spatially and temporally continuous chlorophyll fields are calculated from discontinuous satellite estimates using a new Lagrangian particle-tracing technique for coupling hydrodynamic and biogeochemical models called the property-carrying particle model (PCPM). In this method, tracer particles are initially randomly distributed throughout the computational domain of the hydrodynamic model. For the Lake Superior application, a particle density of 1.2 particles/km^2 was chosen resulting in 100,000 total particles. An initial chlorophyll concentration of 0.6 µg/L on April 1st of each simulation year is assigned to particles, which are distributed randomly in the horizontal and throughout the upper 20 m water column (Fig. 1b). In the Lake Superior model, particles are not allowed to leave the computational domain so the total number of particles remains constant. Particle trajectories are then computed based on 3-D currents computed by the hydrodynamic model. The Lagrangian particle tracking module consists of solving a nonlinear system of ordinary differential equations as follows

$$\frac{dx}{dt} = A(x, t) + B(x, t)\xi(t) \qquad (2)$$

where x is the particle position at a time t, $\frac{dx}{dt}$ is the rate of change of the particle position in time, which is primarily controlled by the 3-dimensional deterministic velocity field, **A**, generated by the model. A random walk-type process has also been added into the 3-D Lagrangian tracking to simulate subgrid-scale turbulent variability in the velocity field represented by stochastic vector **B** with random number ξ, following Visser (1997) and Huret et al. (2007). This equation is solved by the explicit Runge-Kutta multi-step methods. In this version, we have optimized the computational scheme by improving the algorithm for identifying the mesh element which contains a particular particle location. The particle locations are re-initialized on April 1st of each year from 2002–2013, and the hourly locations of the particles are stored for use by PCPM. During the simulation, the particle coverage and density were checked and verified, and no problems with undersampled regions or particle accumulations were found. We do not foresee problems using this technique for longer simulations without re-initialization of the particle position. The PCPM model was re-initialized because we could not run the model for wintertime because a sufficient number of quality satellite images were not available (as in the first paragraph of results section). Therefore, it is not necessary to conduct winter hydrodynamic simulation. Instead, we follow Xue et al. (2015) to simulate the ice-free season and only conduct PCPM from April–October (see justification in the first paragraph of results section).

After the particle trajectories have been calculated (based on the hydrodynamic model grid) and stored, the PCPM employs its own grid system, which is independent of the hydrodynamic model grid. The PCPM grid cells are used only to find the local average chlorophyll concentration from the particles contained within that cell and to transfer information from satellite imagery back to the particles by assimilation. This feature allows PCPM to use a grid resolution appropriate for the satellite data being analyzed, and also allows PCPM to use a more efficient rectilinear grid, even if the particle trajectories were computed from currents on an unstructured grid. For Lake Superior, PCPM uses a 2 × 2 km grid in the horizontal and 10 sigma layers in the vertical for the model domain. Satellite-derived chlorophyll values are interpolated to the PCPM surface layer grid for each available satellite image.

In PCPM, each particle carries a chlorophyll concentration which can change in time. In this application, the evolution of the chlorophyll concentration field is mainly treated as a passive tracer in the hydrodynamic flow field. However, the chlorophyll concentration is dynamically adjusted by assimilation to "nudge" it closer to the satellite estimates at times and locations where imagery is available. The result is a spatially and temporally continuous estimate of the chlorophyll concentration field.

The sequence of operations for each time step in PCPM is as follows:

1. Read particle locations (x, y, z) for all tracer particles at this time step. Locations are pre-computed based on currents from a hydrodynamic model.
2. Determine the PCPM cell for each particle.
3. Calculate PCPM cell-based average of each property. If no particles are present in a particular cell, use the value from the previous time step.
4. Adjust the concentrations of particles within each cell by nudging toward satellite-derived values.
5. Calculate new cell-based average properties for cells containing at least one particle.
6. (Optional) Redistribute cell-based properties to particles within each cell by replacing the particle-based property with a weighted average of the particle-based property and the new cell-based property.
7. Save gridded PCPM concentration field.

In step 4, the concentration of particles in each hydrodynamic grid cell is adjusted at each time step (typically 1 h) to "nudge" the concentration values toward the nearest (in time) satellite-derived value for that cell. The nudging term at time t is:

$$\Delta C = \alpha(C_s - C(t)) \qquad (3)$$

where ΔC is the change in concentration to be applied to $C(t)$. C_s is the remote sensing concentration linearly interpolated to time t from (p)revious and (n)ext. images:

$$C_s = \frac{(t_n - t)C_p + (t - t_p)C_n}{(t_n - t_p)} \qquad (4)$$

where t_n is the time of the next satellite-derived value C_n, and t_p is the time of the previous satellite-derived value C_p. The nudging factor α is:

$$\alpha = \alpha_0 \ max\left(e^{-\left(\frac{t_p - t}{t_0}\right)^2}, e^{-\left(\frac{t_n - t}{t_0}\right)^2} \right) \qquad (5)$$

where t_0 is an adjustable time scaling coefficient and α_0 is an adjustable nudging between 0 and 1. The smaller the value of t_0, the shorter the time that an individual satellite image influences the calculation. The larger the value of α_0, the more strongly the simulated concentration value is steered toward the satellite-derived value. In this study, $\alpha_0 = 0.5$ and $t_0 = 24$ h were used in our standard model simulation, which provided reasonably smooth results. The time window was chosen to be representative of the amount of time it would take a particle to traverse several grid cells (2–5 km) when moving at a typical (2–5 cm/s) current speed. Such a time window is also validated by our decorrelation time scale analysis shown in the later section. We also found that results were not very sensitive to the choice of t_0 and α_0 within a reasonable range, as shown later in our sensitivity analysis. This procedure is carried out for each year (2002 − 2013) with an hourly time step so that at the end of the simulation there are hourly estimates of chlorophyll concentration for each PCPM grid cell.

Results

A total of 2648 MODIS images with at least 10 km² of valid chlorophyll retrievals were available during the 8 Oct. 2002–30 Dec. 2013 period. The climatological average percent of lake area covered per day image for each month was calculated by adding the percent area covered in each image during that month and dividing by 375 (12.5 years times 30 days). The maximum coverages are near 25% for July and August while May, June and September are closer to 15%, with interannual fluctuations of ±5–7% coverage (Fig. 2a). During the early spring in April and early fall in October, the coverage is ~10% while during late fall/winter (November–March) the coverage is below 5% because of increased cloud cover and ice cover. The number of satellite images during these months is <15 per month (Table 1). Thus, a spatial coverage of ~10% of the lake from each image during the winter period makes the average image coverage for the entire lake <5%. Due to extremely low coverage and lower accuracy due to cloud and ice contamination, it is clear that the MODIS-derived data during the November to February period needs to be interpreted with caution and more measurements are needed to validate chlorophyll concentrations during this period of time. For this reason, we exclude data from November to March (Fig. 2b) and re-initialize the model each year in April.

MODIS-derived chlorophyll concentrations were compared to field concentrations measured during USEPA monitoring cruises, which are conducted during spring (mainly in April) and summer (mainly in August) each year. MODIS chlorophyll concentrations exhibit a clear seasonal trend. Chlorophyll values increase during the year from a minimum of about 0.8 μg/L in April, and to a value 1.2 μg/L the late summer and early fall (Fig. 2b). In Lake Superior, most of the EPA sampling stations are in the central basin. Overall, good agreement was found between EPA and MODIS chlorophyll values as indicated by the scatter plot of EPA chlorophyll concentrations and MODIS-derived chlorophyll

concentrations determined from comparisons within 24 h of MODIS imagery (Fig. 3). The average Chlorophyll value for all EPA samples in the comparison is 0.84 μg/L while the average MODIS-derived value is 0.98 μg/L. The correlation coefficient is 0.52 and root-mean-square-error(RMSE) is 0.34 μg/L.

One of the purposes of the interpolation method described in this paper was to use the information contained in spatially and temporally sporadic satellite retrievals to produce a spatially and temporally continuous estimate of chlorophyll concentrations in Lake Superior. The surface chlorophyll fields produced by the interpolation algorithm were used to calculate lake wide and basin-specific climatology of

Table 1
Total days in each month (2002–2013) when MODIS data available.

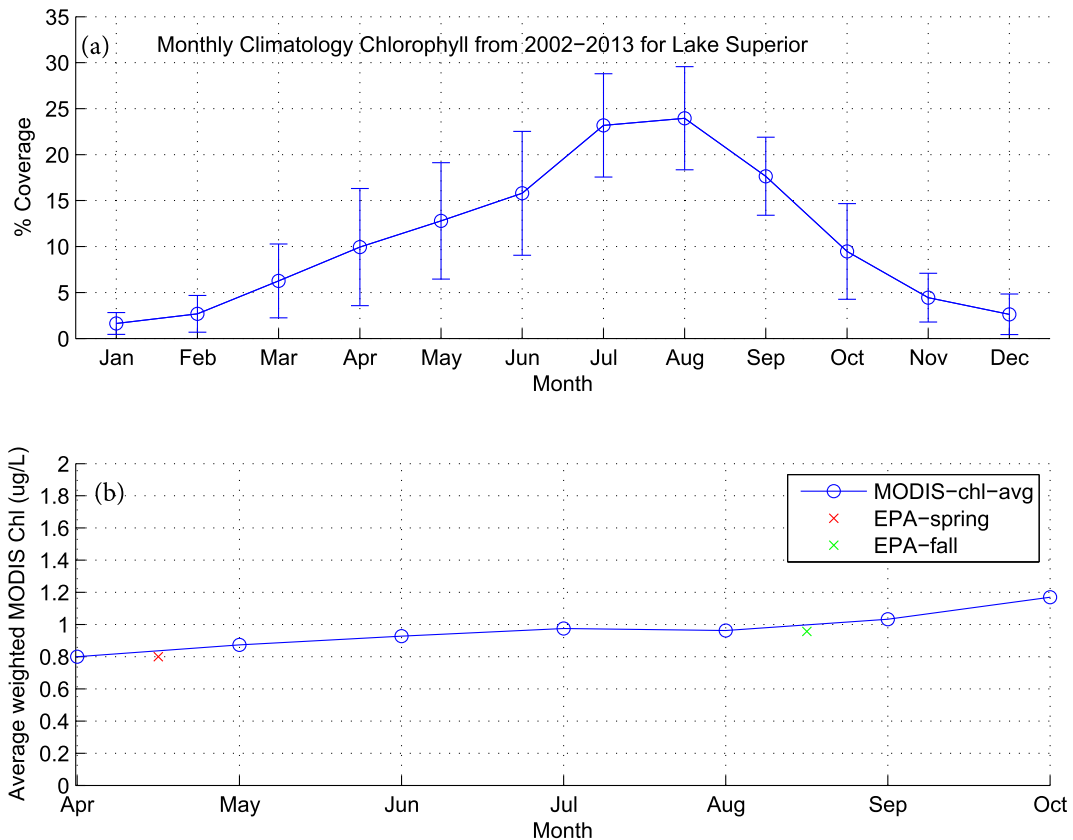| Year	Jan	Feb	Mar	Apr	May	Jun	Jul	Aug	Sep	Oct	Nov	Dec
2002	0	0	0	0	0	0	27	30	28	21	13	17
2003	22	10	14	19	27	33	31	37	26	26	13	24
2004	9	14	21	26	31	34	31	33	33	18	20	11
2005	20	17	31	28	27	35	41	36	25	24	10	8
2006	16	23	28	26	22	34	39	40	33	18	15	21
2007	9	19	24	26	25	35	38	41	22	26	14	14
2008	10	16	24	14	24	28	34	43	24	28	9	13
2009	12	8	13	25	29	31	33	32	35	18	16	9
2010	22	26	24	24	32	27	40	39	32	27	17	16
2011	13	14	25	22	30	28	35	42	32	30	17	12
2012	16	21	23	33	31	33	37	36	35	20	15	9
2013	14	14	28	25	22	25	31	39	32	19	9	14
Average with 2002	14	15	21	22	25	29	35	37	30	23	14	14
Average without 2002	15	17	23	24	27	31	35	38	30	23	14	14

Fig. 2. Upper Panel (a): Average percent coverage per day of MODIS CPA chlorophyll retrievals for Lake Superior, 2002–2013. Lower Panel (b): Average MODIS CPA chlorophyll (weighted by percent coverage) for Lake Superior (April–October), 2002–2013. Crosses indicate average values from EPA spring and summer cruises.
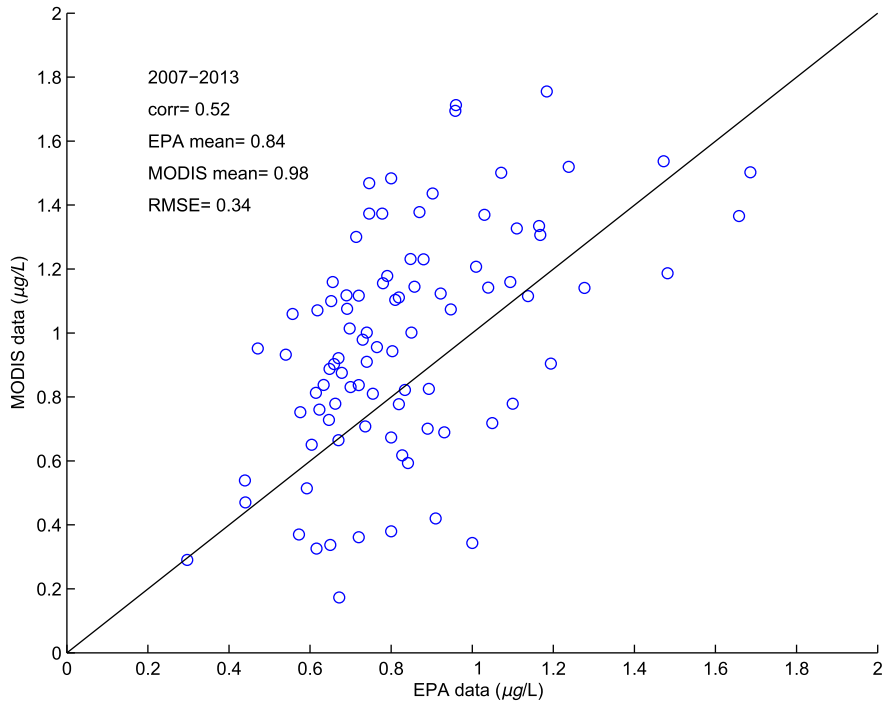
Fig. 3. Observed Lake Superior Chlorophyll from EPA cruises vs. CPA-derived chlorophyll from near coincident (within 24 h) MODIS images. Line is 1:1.

monthly average chlorophyll values (Fig. 4). The lake wide climatological values of monthly average of chlorophyll are similar to the values derived directly from the cruise data for both spring and summer, with relatively larger interannual variability during the fall season. We have also plotted the climatology of monthly average chlorophyll values separately for each of the three Lake Superior basins in Fig. 4. The three basins follow a similar seasonal cycle to the lake wide average with a continual increase in chlorophyll from April to late summer and early fall. The chlorophyll value in the western basin is consistently higher than the lake average by ~0.1 μg/L. The central basin shows a

chlorophyll value lower than lake average by the same amount in the early part of the year while the chlorophyll value in the eastern basin is lower than the lake average after July.

Using our PCPM model, interpolated chlorophyll concentrations can be compared to all individual EPA station chlorophyll concentrations whether they are near coincident (within 24 h) with MODIS images available (89 stations, referred to as NCS stations) or not (another 203 stations). The average Chlorophyll value for all EPA samples in the comparison is 0.89 μg/L and the average value using our method is 0.92 μg/L. Notice that the direct comparison of MODIS and the 89 NCS stations
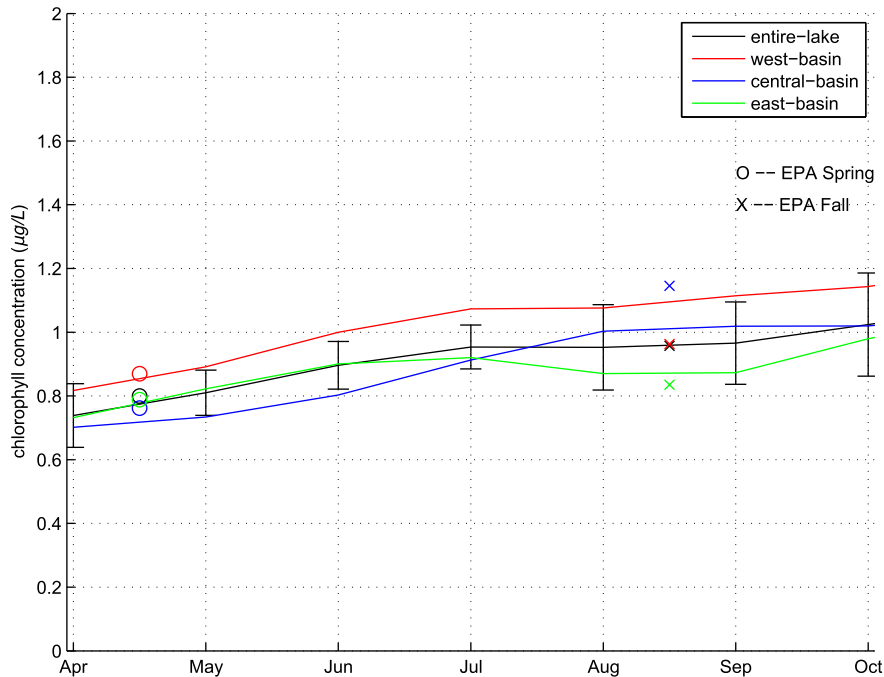

Fig. 4. Climatological value of lakewide average of PCPM interpolated chlorophyll values by month. Circles and Crosses indicate average EPA values for spring and summer cruises. The interannual variability of lakewide average of Chlorophyll values is indicated by standard deviation (black vertical bars).

shows a correlation of 0.52 with a RMSE of 0.34 μg/L (Fig. 3), while the estimates using our approach show even higher correlation with EPA cruise data at the 89 NCS stations with a correlation coefficient of 0.62 with a RMSE of 0.25 μg/L (Fig. 5). Given the errors associated with field sampling in near surface regions and with remote sensed variables on slightly different temporal (hours) and spatial (surface and meters to kilometers), correlations between these type of measurements of 0.5–0.6 are considered good (Fahnenstiel et al., 2016). It is important to note that in most of the EPA cruise cases (203 out of 292), there was not a MODIS-derived value available within 24 h as the EPA sample. Even in these cases, the correlation between the estimates derived from our approach and the EPA cruise data is still 0.48 with a RMSE of 0.31 μg/L. The correlation between all (292) EPA sampling values and our estimates at the stations is 0.50 with a RMSE of 0.30 μg/L (Fig. 5). Both of these comparisons show a similar level of correlation strength and RMSE compared to direct correlation (0.52 RMSE of 0.34 μg/L) between MODIS-derived value and the EPA cruise data at 89 NCS stations (i.e. these differences are not statistically significant). This suggests that results from our approach are very reasonable in producing continuous spatiotemporal estimates of surface chlorophyll concentrations using the PCPM model for interpolation.

The spatial variation in interpolated chlorophyll concentrations for different seasons is illustrated in Fig. 6. The maps show relatively higher chlorophyll concentration in the southern nearshore regions and embayments of the western and eastern basins during April–June (Spring), particularly in Duluth Bay, Whitefish Bay and the southern coasts of the western basin with a chlorophyll anomaly ~1 μg/L higher than the lake-mean value. Also, along the northern coasts, higher chlorophyll concentrations were found in Thunder Bay. In contrast, the chlorophyll concentration in the offshore waters remains relatively low in all three basins of Lake Superior. In July–September (summer), the patterns are quite similar in Duluth Bay and Thunder Bay, characterized with much higher chlorophyll concentration. The chlorophyll concentration in Whitefish Bay is still higher than offshore water but lower than that in the other bays. A noticeable difference between spring and summer is higher chlorophyll concentration along the southern coasts of the western

basin, where the chlorophyll concentration becomes quite low during summer time in comparison to spring (e.g. Keweenaw coast). Although the chlorophyll concentration in offshore water is generally low, the northern central basin shows a relatively higher concentration during summer in comparison to spring. For the fall seasons, relatively higher values of chlorophyll are again seen in the southwest part of the western basin and the embayments, but with somewhat lower spatial gradients.

The mean annual chlorophyll concentrations for specific regions of the lake during the 2002–2013 period are presented in Fig. 7. The lake wide mean varies between 0.8 μg/L and 1.0 μg/L during the simulated period of time with a slight increasing trend of 0.005 μg/yr, however, the *P*-value of 0.576 (≫ 0.05), suggests the rate is not statistically significant and there is no clear increasing or decreasing trend in lake wide mean concentration. On the other hand, the chlorophyll concentrations in the embayment waters show much higher inter-annual variability. In the Duluth Bay, the chlorophyll concentration varies between 1.4 μg/L–1.8 μg/*L* with a much higher mean value of 1.6 μg/L, representing the highest chlorophyll concentration in Lake Superior. The chlorophyll concentration in Thunder Bay, Whitefish Bay and the southern coasts of the western basin are also higher than in offshore waters, but there was no clear time correlation of the inter-annual pattern among these embayment waters.

As an example of the analysis that can be performed on the continuous spatio-temporal estimates, which would be difficult or impossible with the raw satellite images, we calculated the autocorrelation function at each grid square in the interpolated images for each year with data from April–October (2003 − 2013). The autocorrelation function gives an indication of the persistence of a value in time. It has a value of 1 for a time lag of 0 and generally falls off with increasing time lag. The decorrelation time is usually defined as the time lag at which the autocorrelation function falls below $1/e$ ($= 0.368$). Fig. 8 is a map of the average decorrelation time scale from the 11 years with data of April–October. It shows areas of more persistence (>10 days) in the center of the central basin and in the embayments. There is lower persistence (more variability) in a 15–20 km band around the Keweenaw Peninsula of the western basin, at the northern coast of the central
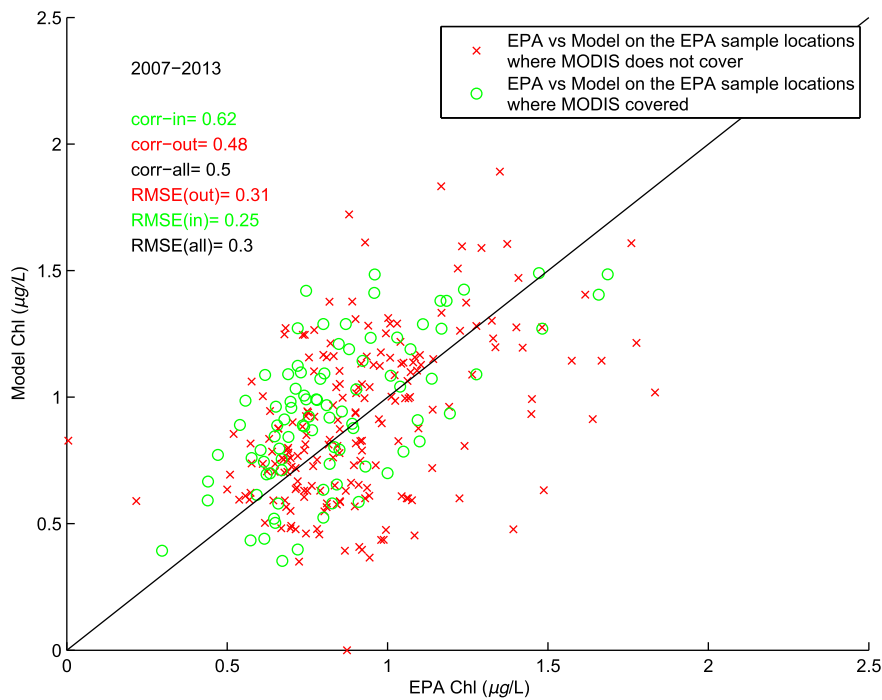

Fig. 5. Observed Lake Superior chlorophyll from EPA cruises vs. chlorophyll estimated from PCPM interpolated approach for 2007–2013. There are 89 EPA sampling stations that have near coincident (within 24 h) MODIS images available (referred to as NCS stations using open circles) and 203 other stations (OS indicated with crosses) that have not near coincident MODIS images available, with total 292 stations (TS). Solid line is 1:1 line.
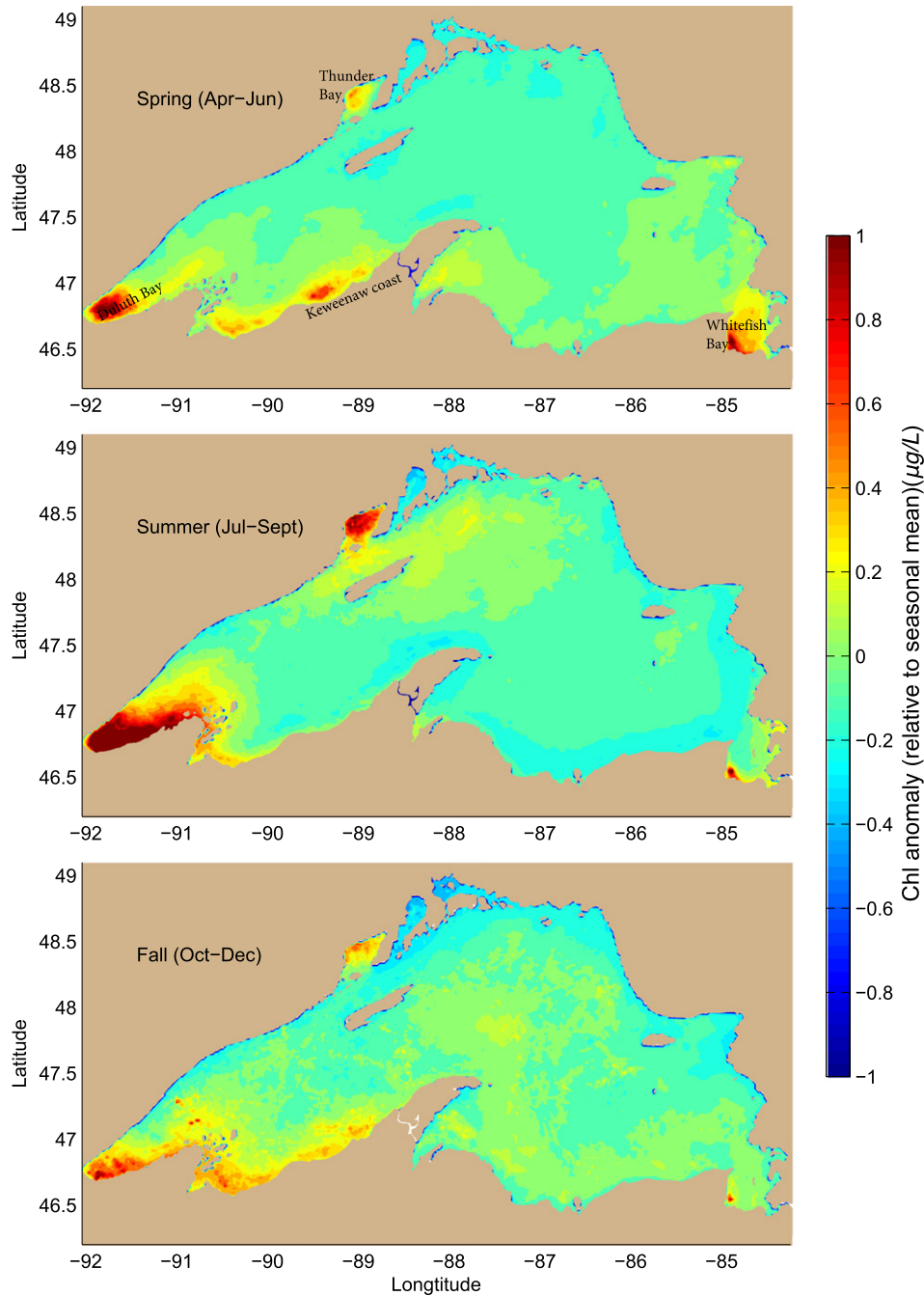
Fig. 6. Chlorophyll concentration anomalies from PCPM estimation.

basin, and in the entire eastern basin. This map should be interpreted in conjunction with Fig. 6 since high variability in areas of low average chlorophyll concentration may not be as important as high variability in areas of high chlorophyll concentration.

Fig. 9 is a graph of the fraction of the lake surface for which the decorrelation time exceeds a particular value. It shows that the decorrelation time is longer than 5 days in nearly the entire lake, but 70% of the lake has decorrelation time scale between 5 and 10 days, consistent with phytoplankton growth rates (Fahnenstiel et al., 2000). In <25% of the lake, the decorrelation time scale exceeds 10 days, which is indicative of weaker flow and resulting longer residence time in those areas. Thus, satellite images may not realistically characterize lake conditions after 10 days. Based on the 11 year autocorrelation

analysis, satellite retrievals of Lake Superior water quality parameters are representative of actual water conditions for approximately a week ± 3 days, with the exception of a few nearshore areas. To examine the sensitivity of the decorrelation time scale to the choice of the nudging parameter, we repeated the PCPM simulation with other different nudging coefficients $\alpha_0 = 0.1$, 0.2 and 1 and $t_0 = 12$ h, 36 h, 48 h (Fig. 9). The estimated decorrelation time scale showed no significant change. This provides us with some confidence that the estimated decorrelation time scale is a robust dynamic feature and not a parameter-dependent artifact.

To assess the impact of the hydrodynamic transport on chlorophyll distribution, we conducted a second experiment (here referred to as Ex#2) in which the particles stay fixed at their initial position. In other

Fig. 7. Lakewide annual mean chlorophyll with PCPM interpolated approach. Crosses are averages from EPA spring and summer cruises for each year. Chlorophyll estimates for Duluth bay and average of Thunder Bay (TB), Whitefish Bay (WB) and South Coast (SC) of the western basin are also presented. Open circles are averages from PCPM interpolated estimates at same locations as EPA data in spring and summer.

words, the chlorophyll field is updated based only on satellite data, without advection from the hydrodynamic model. Fig. 10 shows the difference in chlorophyll spatial pattern estimated from standard PCPM simulation (here referred to as reference experiment) and Ex#2. Results show that the major differences occur in the coastal waters, where coastal currents are much stronger in comparison to weaker offshore currents (Fig. 15 in Xue et al., 2015). During spring and summer, the largest differences occur on the south coast in the western basin from Duluth Bay through the Keweenaw Peninsula as well as in the Whitefish Bay on the eastern coast and Thunder Bay on the northern coast. For example, increased chlorophyll concentration is observed near the coast in

Duluth Bay in the standard PCPM simulation along with the decreased concentration in offshore water within the bay, which reflects the fine scale aggregation and redistribution of chlorophyll influenced by the coastal jet transport. A similar influence of coastal currents on chlorophyll concentration is clearly shown in other coastal waters. During the fall season, the general spatial pattern of the difference in chlorophyll concentration between the two experiments is similar with a larger difference observed in the central basin in comparison to the spring and summer cases. As expected, there are no significant changes in the mid-lake due to the lower impact of weaker offshore water flow and large, direct influence from nudging of the satellite image.
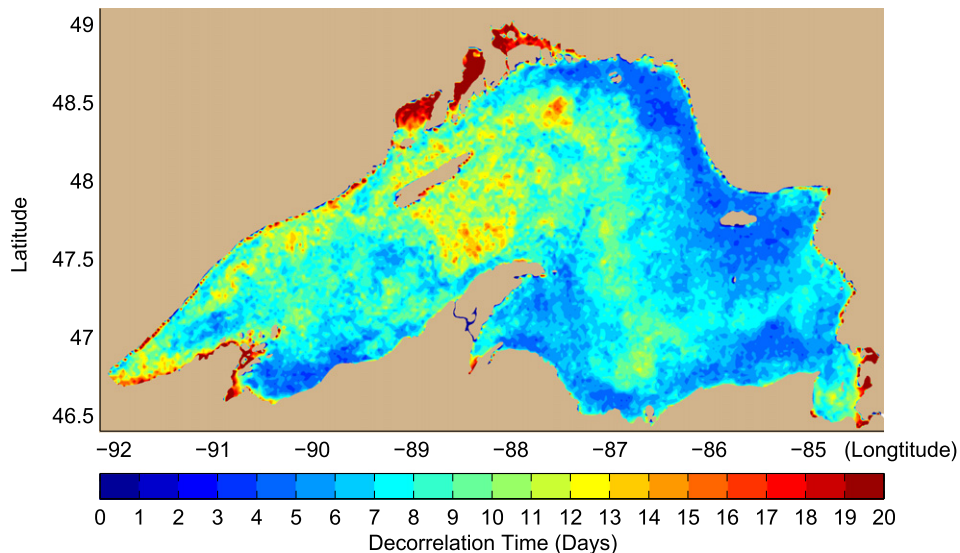

Fig. 8. Map of average decorrelation time scale for the April–October period, 2003–2013.
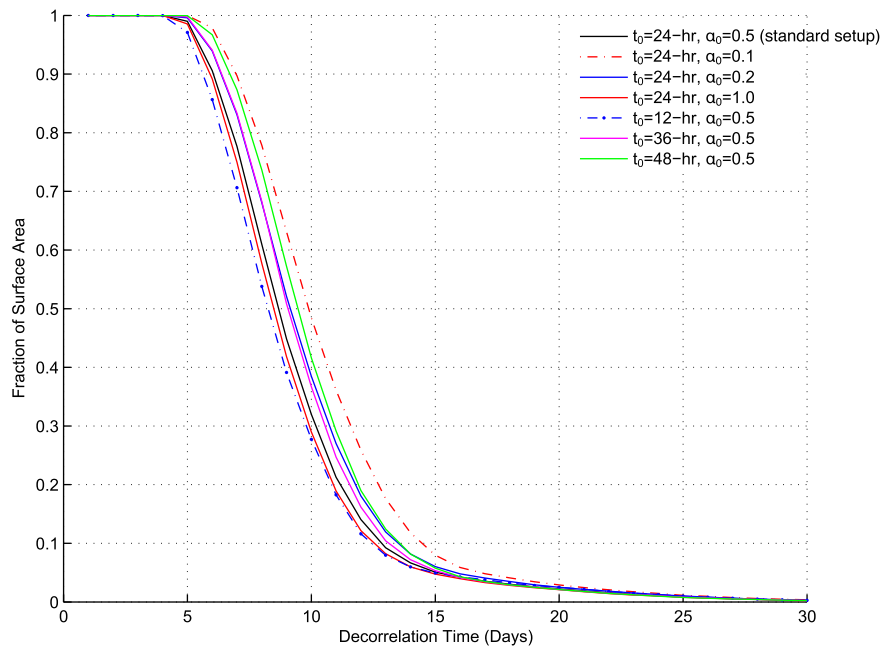
Fig. 9. Fraction of Lake Superior surface area which exceeds a given decorrelation time scale, sensitivity analysis is conducted with various nudging coefficients.

Unfortunately, because there are no observational data available for us to quantitatively evaluate the model performance in coastal waters, we cannot definitively demonstrate the improvement in the PCPM model with advection over the case with no advection, but the differences observed in the two experiments do serve to reflect the importance of hydrodynamics on the spatio-temporal distribution of biological parameters in the coastal region.

Discussion and conclusions

Model novelty

In this paper, we describe a novel method for providing objective estimates of spatially and temporally continuous distribution of a satellite-derived water property with an application to the estimates of chlorophyll concentration in Lake Superior. The novelty of this new technique lies in its integration of hydrodynamic effects via the property-carrying particle tracking model and Eulerian concentration remapping approach, which allow the model to reconstruct continuous spatial fields with extremely high flexibility and efficiency consistent with hydrodynamic constraints. Compared to traditional objective mapping, a significant advantage is that our method allows the continuous dynamic evolution of the fields over time driven by hydrodynamic conditions to resolve the transport and mixing processes. This is extremely important in the regions characterized by strong currents and short residence time as biological properties may be dominated by advective transport rather than local biogeochemical processes. Many studies (see Xue et al., 2017 have demonstrated that the 1-D vertical processes (primarily mixing and eddy diffusivity) are insufficient to characterize the hydrodynamic conditions of the Great Lakes and horizontal transport must be resolved due to their sea-like characteristics. In addition, the traditional mapping scheme is generally not able to determine the distribution pattern on the local scale as it mainly relies on the interpolation of observations, while the particle tracking program allows for representation of much smaller dynamic scales such as steep gradients at fronts.

Our approach offers significant improvements over traditional tracer-based modeling approaches. Compared to the traditional tracer-based model that could have been used to resolve the effect of water transport and mixing on the chlorophyll concentration, PCPM is simpler to implement (no need to solve the concentration equation on the hydrodynamic grid) and more efficient (can use its own rectilinear grid system, independent of the hydrodynamic grid). For example, the 12-year (2002–2013) hydrodynamic simulation takes 20 days to complete using 64 CPUs; in the second step, the particle tracking model used to generate the particle trajectories takes ~96 h using 64 CPUs; however, in step 3, the PCPM can complete its 12-year simulation using the particle trajectories as input within 30 min using a single CPU. Note that Step 1 (hydrodynamic simulation) and step 2 (the particle trajectory generations) will be run only once regardless of property's concentration because the hydrodynamics and associated water transport and mixing (represented by the hundreds of thousands of particle trajectories) are not affected by biochemical properties (in this case, chlorophyll fields). In other words, we only need to run the step 3-PCPM offline with necessary modifications for different sets of parameters and property configurations. This would be extremely useful, for instance, if one conducts Monte-Carlo types of simulations, or wants to simulate other property fields (e.g. contaminant spill, phosphorus concentration etc.) using only 30 min per run. Such a high level of efficiency is not available from tracer-based models because one will have to re-run the tracer-tracking model (similar to our step 2) for any change in parameter configuration or estimation of different property concentration. Furthermore, our model converts the particle properties back to an Eulerian grid mesh, which significantly reduces the required particle numbers and avoids any singularity of the estimated fields.

More importantly, the integration of Lagrangian and Eulerian approaches allows a very natural coupling of mass transport (represent by particle movements and random walk) and biological processes in water columns, which can often be described by a common vertical 1-D biological model (e.g. Nutrient-Plankton-Zooplankton-Detritus model). In this study, the sinks and sources of chlorophyll are implicitly represented by the assimilation of the satellite imagery. Our next goal is to use the same PCPM particle-tracking framework for spatial and temporal interpolation of satellite images, to couple with a 1-D NPZD model for each grid-based water column and form a 3-D biological model. We
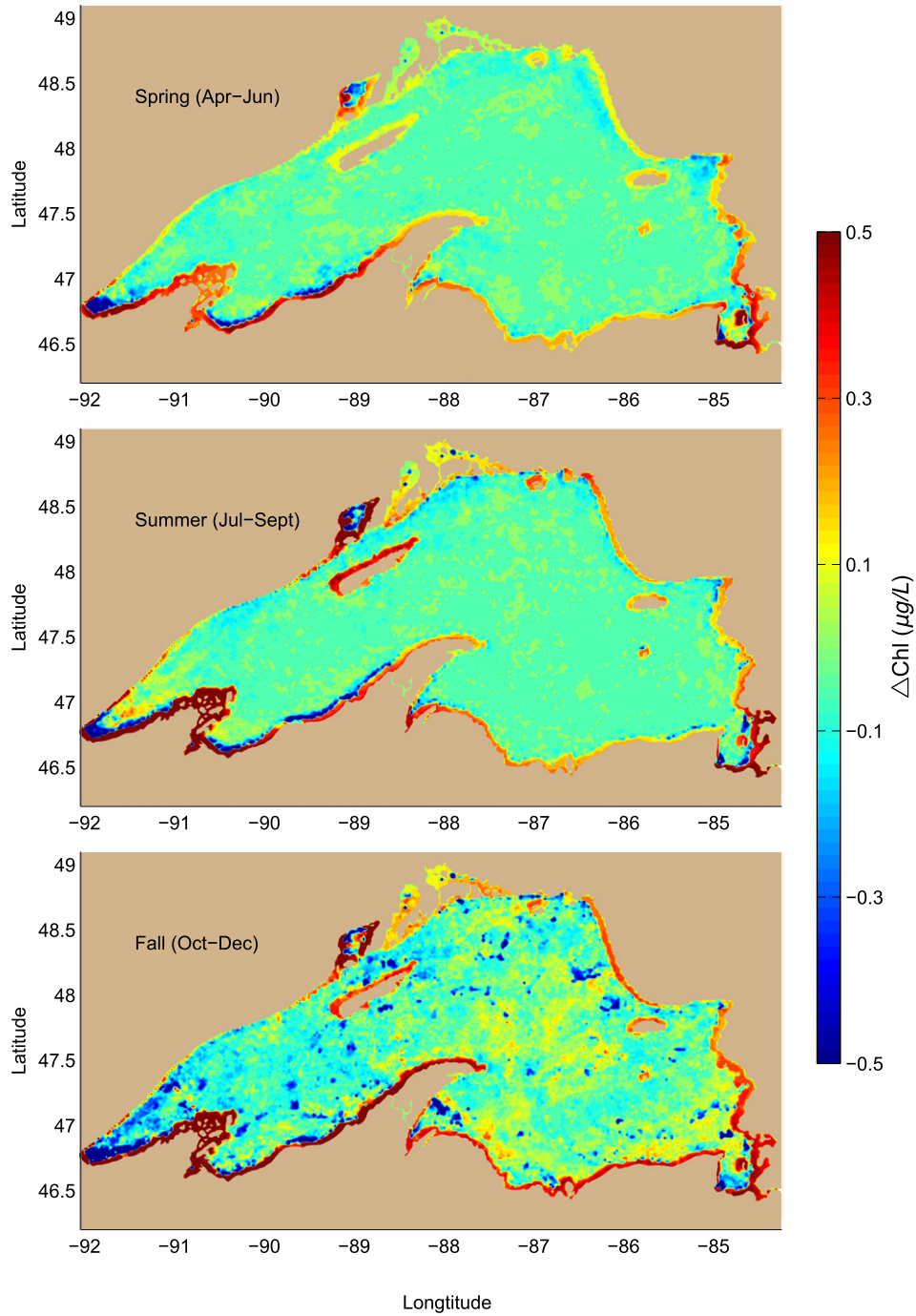
Fig. 10. The difference in chlorophyll spatial pattern between the standard PCPM simulation (i.e. reference experiment) and Ex#2.

expect the PCPM model to be far more efficient than traditional tracer-based Eulerian bio-physical models for 3-D simulation for the same reason discussed above.

Lake Superior chlorophyll pattern and associated hydrodynamic constraints

An important characteristic revealed from the analysis is the seasonally-dependent chlorophyll concentration, which is consistent with seasonal hydrodynamic conditions in Lake Superior (Chen et al., 2001; Xue et al., 2015). The western basin is known for earlier spring warming compared to other basins, so the biological productivity in Duluth Bay and the southern coasts in the western basin starts earlier than in other regions. During spring, the coastal currents have not fully developed near the southern coast due to easterly wind and homogeneous water temperature. This allows the high chlorophyll concentration to temporarily persist along the southern coasts in the western basin. During the summer time, the chlorophyll concentration continues to increase in the embayments while the concentration near the southern coasts become much lower, which is associated with the formation and intensification of the coastal jet current (Chen et al., 2001). In summer, southwesterly winds prevail along the southern coasts of the western basin, which favors the development of longshore currents. In addition, the strongest spatial thermal gradients form near the Keweenaw Peninsula and the density-driven flow intensifies the coastal jet currents (Beletsky et al., 1999; Xue et al., 2015). These hydrodynamic changes cause exceptionally strong mass transport and low residence time, resulting in low chlorophyll concentration in this region compared to spring.

While EPA cruise data are primarily designed to sample the off-shore water, our model provides new insights in the observational sampling design. Our estimates of the long-term spatial distribution of chlorophyll concentration show that there are no significant differences in magnitude and trend in three basins, similar to the findings reported by Fahnenstiel et al. (2016). Furthermore, our analyses suggest the necessity for enhanced sampling in the embayments and coastal waters, where the chlorophyll concentration is considerably higher than the lake wide average (up to 80%) Without adding extra cost, moving a few sampling locations from offshore water to embayments and southern coastal regions can provide more accurate characterization of the spatial pattern of chlorophyll concentration in Lake Superior.

Lake Superior chlorophyll temporal trend and associated ecological significance

Our new lake-wide annual chlorophyll concentrations based on the particle tracking approach are similar to those determined from similar remote sensing algorithms for the 2010–2013 period, and provide some confidence for our results. Fahnenstiel et al. (2016) reported a mean lake-wide chlorophyll concentration of 0.99 μg/L, which compares favorably to our mean of 0.97 μg/L for the same period.

Lake Superior chlorophyll concentrations do not appear to have changed significantly over the past 12 years, and only slightly or not at all over the last ~50 years. Based on our analysis, annual lake-wide chlorophyll concentrations averaged 0.8–1.0 μg/L in 2003–2013 with overall mean of 0.94 μg/L and offshore or open water concentrations averaged 0.92 μg/L during this same period (Fig. 7). In a review of phytoplankton biomass concentrations in the Great Lakes prior to 1974, Vollenweider et al. (1974) reported that open lake concentrations in Lake Superior were <1 μg/L and nearshore values were higher. Schelske and Roth (1973) reported a mean concentrations of chlorophyll *a* in the open lake region of Lake Superior to be 0.7 μg/L in 1970 which is similar to the offshore concentrations in 1980/81 reported by Nalewajko and Voltolina (1986). In a lake-wide sampling (114–144 stations per cruise) of Lake Superior during six cruises (May–November) in 1973, Watson et al. (1975) reported a mean annual chlorophyll *a* concentration for Lake Superior of 1.1 μg/L. Given the variability associated with these historical samplings and the relative similarity among historical values, it is reasonable to suggest that lake wide chlorophyll concentrations have changed very little in Lake Superior over the last ~50 years.

The similarity of chlorophyll concentrations in Lake Superior over the last 15 years is in marked contrast to the trends that have been observed in lakes Huron and Michigan. In lakes Michigan and Huron large changes in chlorophyll concentrations and many other water quality parameters have been noted in the past 15 years or so. Winter/spring chlorophyll concentrations have decreased from 30 to 75% in the last 15–20 years in lakes Michigan and Huron (Fahnenstiel et al., 2010; Barbiero et al., 2011; Warner and Lesht, 2015). These chlorophyll decreases were accompanied by decreases in diatom production and total phosphorus concentrations with the result that chlorophyll and phosphorus concentrations are now relatively similar among all three of the Upper Great Lakes (Mida et al., 2010; Barbiero et al., 2012). Moreover, the changes in lakes Huron and Michigan chlorophyll concentration likely extend back into the early 1970s as Fahnenstiel et al. (2016) noted that lakes Huron and Michigan chlorophyll in 2010–2013 has decreased over 50% from early 1970 values.

The large changes in chlorophyll concentrations in lakes Huron and Michigan during the past 15 years or so are most likely due to the filtering activities of invasive mussels (Fahnenstiel et al., 2010; Mida et al., 2010; Kerfoot et al., 2010; Vanderploeg et al., 2010; Evans et al., 2011; Yousef et al., 2014; Rowe et al., 2015), although other factors (phosphorus and climate change) may play a role (Warner and Lesht, 2015).

Large populations of dreissenid mussels, particularly *Dreissenia rostriformis bugenis*, became established in the Upper Great Lakes in the 2000s (Nalepa et al., 2010) and their high abundances and filtering rates have been related to significant declines in chorophyll concentrations in Lake Michigan (Fahnenstiel et al., 2010; Vanderploeg et al., 2010; Rowe et al., 2014). Also, phosphorus is the limiting nutrient in the Upper Great Lakes and concentrations of chlorophyll have been related to phosphorus concentrations (Schelske et al., 1974; Scavia et al., 1986). Phosphorus load reductions were initiated in the Great Lakes in the 1970s with the result that loading has decreased in the Great lakes over the last 30 years (Dolan and Chapra, 2012) and these decreases may have affected chlorophyll concentrations (Warner and Lesht, 2015). Finally, in the past few decades, climate change has altered Great Lakes water temperatures and lengthened the period of thermal stratification (McCormick and Fahnenstiel, 1999; Austin and Colman, 2007). Climate change has been suggested as an important factor in resurgence of cyanobacteria blooms in western Lake Erie (Michalak et al., 2013) and possibly in controlling chlorophyll concentrations in lakes Huron and Michigan (Warner and Lesht, 2015).

The difference in chlorophyll trends among the Upper Great Lakes during the past 15 years reflects the relative role of these stressors, dreissenid mussels and nutrient loading in each lake. In contrast to lakes Huron and Michigan, dreissenid mussels and changes in phosphorus loads have likely not impacted the Lake Superior ecosystem, and are consistent with the lack of a chlorophyll trend in the past 15 years. Lake Superior, unlike lakes Huron and Michigan, has very few dreissenid mussels (Grigorovich et al., 2008) an observation which has been related to the low calcium concentrations in the lake (Grigorovich et al., 2003). Moreover, phosphorus loadings have not changed in Lake Superior for the period 1980–2010, whereas loadings have decreased between 17 and 40% in lakes Michigan and Huron over the same period (Dolan and Chapra, 2012). The lack of mussels and no change in phosphorus loading should produce relatively similar chlorophyll concentrations over the last 15 years and possibly longer, and this is what we observed.

Climate change is another factor that might affect chlorophyll concentrations in the Great Lakes (O'Reilly et al., 2015; Warner and Lesht, 2015), although the exact mechanism may be unclear. Climate change can affect chlorophyll concentrations through a variety of mechanisms including the length and intensity of thermal stratification, duration and extent of ice cover, and frequency and intensity of storms (Michalak et al., 2013; Scavia et al., 1986; Shimoda et al., 2011). Because the climate is changing in the Lake Superior region (McCormick and Fahnenstiel, 1999; Austin and Colman, 2007) there is the potential for significant effects on chlorophyll concentrations. Fahnenstiel et al. (2016) noted a relationship between summer temperatures and summer phytoplankton productivity in Lake Superior for the period 2010–2013. On an annual basis, we did not detect a statically significant change in Lake Superior annual temperature (GLSEA data) or chlorophyll concentrations for the period of 2002–2013. The lack of trends in either variable found in this study should not be used as an indicator of no climate effect. Rather, our limited observation period (12 years), and limited analysis (annual chlorophyll and temperature only) may have masked more subtle effects. Because Lake Superior is sensitive to temperature change (i.e., ice cover, limited period of thermal stratification, etc.), future studies on the relationships between climate and phytoplankton abundance should be encouraged.

Acknowledgements

References

Ackerman, S.A., Heidinger, A., Foster, M.J., Maddux, B., 2013. Satellite regional cloud climatology over the Great Lakes. Remote Sens. 5 (12), 6223–6240.

Anderson, E.J., Schwab, D.J., 2013. Predicting the oscillating bi-directional exchange flow in the Straits of Mackinac. J. Great Lakes Res. 39, 663–671.

Austin, J.A., Colman, S.M., 2007. Lake Superior summer water temperatures are increasing more rapidly than regional air temperatures: a positive ice-albedo feedback. Geophys. Res. Lett. 34, L06604.

Barbiero, R.P., Lesht, B.M., Warren, G.J., 2011. Evidence for bottom–up control of recent shifts in the pelagic food web of Lake Huron. J. Great Lakes Res. 37, 78–85.

Barbiero, R.P., Lesht, B.M., Warren, G.J., 2012. Convergence of trophic state and the lower food web in Lakes Huron, Michigan and Superior. J. Great Lakes Res. 38, 368–380.

Beletsky, D., Saylor, J.H., Schwab, D.J., 1999. Mean circulation in the Great Lakes. J. Great Lakes Res. 25, 78–93.

Bennington, V., McKinley, G.A., Kimura, N., Wu, C.H., 2010. General circulation of Lake Superior: mean, variability, and trends from 1979 to 2006. J. Geophys. Res. Oceans 115, C12015.

Chen, C., Beardsley, R.C., Cowles, G., 2006. An unstructured grid, finite-volume coastal ocean model (FVCOM) system. Oceanography 19, 78–89.

Chen, C., Xu, Q., Houghton, R., Beardsley, R.C., 2008. A model-dye comparison experiment in the tidal mixing front zone on the southern flank of Georges Bank. J. Geophys. Res. 113, C02005. http://dx.doi.org/10.1029/2007JC004106.

Chen, C., Zhu, J., Ralph, E., Green, S.A., Budd, J.W., Zhang, F.Y., 2001. Prognostic modeling studies of the Keweenaw current in Lake Superior. Part I: formation and evolution. J. Phys. Oceanogr. 31, 379–395.

Dolan, D.M., Chapra, S.C., 2012. Great Lakes total phosphorus revisited: 1. Loading analysis and update (1994–2008). J. Great Lakes Res. 38, 730–740.

Dupont, F., Chittibabu, P., Fortin, V., Rao, Y.R., Lu, Y., 2012. Assessment of a NEMO-based hydrodynamic modelling system for the Great Lakes. Water Qual. Res. J. Can. 47, 198–214.

Evans, D.O., Skinner, A.J., Allen, R., McMurtry, M.J., 2011. Invasion of zebra mussel, Dreissena polymorpha, in Lake Simcoe. J. Great Lakes Res. 37 (Supplement 3), 36–45.

Fahnenstiel, G.L., Stone, R.A., McCormick, M.J., Schelske, C.L., Lohrenz, S.E., 2000. Spring isothermal mixing in the Great Lakes: evidence of nutrient limitation in a sub-optimal light environment. Can. J. Fish. Aquat. Res. 57, 1901–1910.

Fahnenstiel, G., Pothoven, S., Vanderploeg, H., Klarer, D., Nalepa, T., Scavia, D., 2010. Recent changes in primary production and phytoplankton in the offshore region of southeastern Lake Michigan. J. Great Lakes Res. 36 (Supplement 3), 20–29.

Fahnenstiel, G.L., Sayers, M.J., Shuchman, R.A., Yousef, F., Pothoven, S.A., 2016. Lake-wide phytoplankton production and abundance in the Upper Great Lakes: 2010–2013. J. Great Lakes Res. 42, 619–629.

Grigorovich, I.A., Koniushin, A.V., Gray, D.K., Duggan, I.C., Colautti, R.I., MacIsaac, H.J., 2003. Lake Superior: an invasion coldspot. Hydrobiologie 499, 191–210.

Grigorovich, I.A., Kelly, J.R., Darling, J.A., West, C.W., 2008. The quagga mussel invades the Lake Superior Basin. J. Great Lakes Res. 34, 342–350.

Huret, M., Runge, J.A., Chen, C., Cowles, G., Xu, Q., Pringle, J.M., 2007. Dispersal modeling of fish early life stages: sensitivity with application to Atlantic cod in the western Gulf of Maine. Mar. Ecol. Prog. Ser. 347, 261–274.

Johengen, T.H., Johannsson, O.E., Pernie, G.L., Millard, E.S., 1994. Temporal and spatial trends in nutrient dynamics and biomass measures in lakes Michigan and Ontario in response to phosphorus control. Can. J. Fish. Aquat. Sci. 51, 2570–2578.

Kerfoot, W.C., Yousef, F., Green, S.A., Budd, J.W., Schwab, D.J., Vanderploeg, H.A., 2010. Approaching storm: disappearing winter bloom in Lake Michigan. J. Great Lakes Res. 36 (Supplement 3), 30–41.

Lehman, J.T., 1988. Algal biomass unaltered by food-web changes in Lake Michigan. Nature 332, 537–538.

Makarewicz, J.C., Bertram, P., 1991. Evidence for the restoration of the Lake Erie ecosystem. Bioscience 41, 216–223.

McCormick, M.J., Fahnenstiel, G.L., 1999. Recent climatic trends in nearshore water temperatures in the St. Lawrence Great Lakes. Limnol. Oceanogr. 44, 530–540.

Michalak, A.M., et al., 2013. Record-setting algal bloom in Lake Erie caused by agricultural and meteorological trends consistent with expected future conditions. Proc. Natl. Acad. Sci. 110, 6448–6452.

Mida, J.L., Scavia, D., Fahnenstiel, G.L., Pothoven, S.A., Vanderploeg, H.A., Dolan, D.M., 2010. Long-term and recent changes in southern Lake Michigan water quality with implications for present trophic status. J. Great Lakes Res. 36 (Supplement 3), 42–49.

Nalepa, T.F., Fanslow, D.L., Pothoven, S.A., 2010. Recent changes in density, biomass, recruitment, size structure, and nutritional state of Dreissena populations in southern Lake Michigan. J. Great Lakes Res. 36 (Supplement 3), 5–19.

Nalewajko, C., Voltolina, D., 1986. Effects of environmental variables in growth rates and physiological characteristics of Lake Superior phytoplankton. Can. J. Fish. Aquat. Sci. 43, 1163–1170.

National Center for Atmospheric Research. 2015 Last modified 20 Oct 2015. The climate data guide: climate forecast system reanalysis (CFSR). Retrieved from https://climatedataguide.ucar.edu/climate-data/climate-forecast-system-reanalysis-cfsr.

O'Reilly, C.M., et al., 2015. Rapid and highly variable warming of lake surface waters around the globe. Geophys. Res. Lett. 42 (2015GL066235).

Rowe, M.D., Kreis Jr., R.G., Dolan, D.M., 2014. A reactive nitrogen budget for Lake Michigan. J. Great Lakes Res. 40, 192–201.

Rowe, M.D., Anderson, E.J., Wang, J., Vanderploeg, H.A., 2015. Modeling the effect of invasive quagga mussels on the spring phytoplankton bloom in Lake Michigan. J. Great Lakes Res. 41 (Supplement 3), 49–65.

Saha, S., et al., 2010. The NCEP climate forecast system reanalysis. Bull. Am. Meteorol. Soc. 91, 1015–1057.

Scavia, D., Fahnenstiel, G.L., Evans, M.S., Jude, D.J., Lehman, J.T., 1986. Influence of salmon predation and weather on long-term water quality trends in Lake Michigan. Can. J. Fish. Aquat. Sci. 43, 435–443.

Schelske, C.L., Roth, J.C., 1973. Limnological Survey of Lakes Michigan, Superior, Huron and Erie. Great Lakes res. Div. Publ #17. Univ. Michigan, Ann Arbor, MI.

Schelske, C.L., Rothman, E.D., Stoermer, E.F., Santiago, M.A., 1974. Response of phosphorus limited Lake Michigan phytoplankton to factorial enrichment of nitrogen and phosphorus. Limnol. Oceanogr. 19, 409–419.

Schwab, D.J., Bedford, K.W., 1994. Initial implementation of the Great Lakes forecasting system: a real-time system for predicting lake circulation and thermal structure. Water Pollut. Res. J. Canada 29, 203–220.

Schwab, D.J., Leshkevich, G.A., Muhr, G.C., 1999. Automated mapping of surface water temperature in the Great Lakes. J. Great Lakes Res. 25, 468–481.

Shimoda, Y., Azim, M.E., Perhar, G., Ramin, M., Kenney, M.A., Sadraddini, S., Gudimov, A., Arhonditsis, G.B., 2011. Our current understanding of lake ecosystem response to climate change: what have we really learned from the north temperate deep lakes? J. Great Lakes Res. 37, 173–193.

Shuchman, R.A., Leshkevich, G., Sayers, M.J., Johengen, T.H., Brooks, C.N., Pozdnyakov, D., 2013. An algorithm to retrieve chlorophyll, dissolved organic carbon, and suspended minerals from Great Lakes satellite data. J. Great Lakes Res. 39 (Supplement 1), 14–33.

Vanderploeg, H.A., Liebig, J.R., Nalepa, T.F., Fahnenstiel, G.L., Pothoven, S.A., 2010. Dreissena and the disappearance of the spring phytoplankton bloom in Lake Michigan. J. Great Lakes Res. 36 (Supplement 3), 50–59.

Visser, A.W., 1997. Using random walk models to simulate the vertical distribution of particles in a turbulent water column. Mar. Ecol. Prog. Ser. 158, 275–281.

Vollenweider, R.A., Munawar, M., Stadelmann, P., 1974. A comparative review of phytoplankton and primary production in the Laurentian Great Lakes. J. Fish. Res. Board Can. 31, 739–762.

Warner, D.M., Lesht, B.M., 2015. Relative importance of phosphorus, invasive mussels and climate for patterns in chlorophyll a and primary production in Lakes Michigan and Huron. Freshw. Biol. 60, 1029–1043.

Watson, N.H.F., Thomson, K.P.B., Elder, F.C., 1975. Sub-thermocline biomass concentration detected by transmissometer in Lake superior. Verh. Int. Verein Limnol. 19, 682–688.

White, B., Austin, J., Matsumoto, K., 2012. A three-dimensional model of Lake Superior with ice and biogeochemistry. J. Great Lakes Res. 38, 61–71.

Xue, P., Chen, C., Ding, P., Beardsley, R.C., Lin, H., Ge, J., Kong, Y., 2009. Saltwater intrusion into the Changjiang River: a model-guided mechanism study. J. Geophys. Res. Oceans 114, C02006.

Xue, P., Schwab, D.J., Hu, S., 2015. An investigation of the thermal response to meteorological forcing in a hydrodynamic model of Lake Superior. J. Geophys. Res. Oceans 120, 5233–5253.

Xue, P., Pal, J.S., Ye, X., Lenters, J.D., Huang, C., Chu, P.Y., 2017. Improving the simulation of large lakes in regional climate modeling: two-way lake-atmosphere coupling with a 3-D hydrodynamic model of the Great Lakes. J. Clim. 30:1605–1627. http://dx.doi.org/10.1175/JCLI-D-16-0225.1.

Yousef, F., Charles Kerfoot, W., Shuchman, R., Fahnenstiel, G., 2014. Bio-optical properties and primary production of Lake Michigan: insights from 13-years of SeaWiFS imagery. J. Great Lakes Res. 40, 317–324.